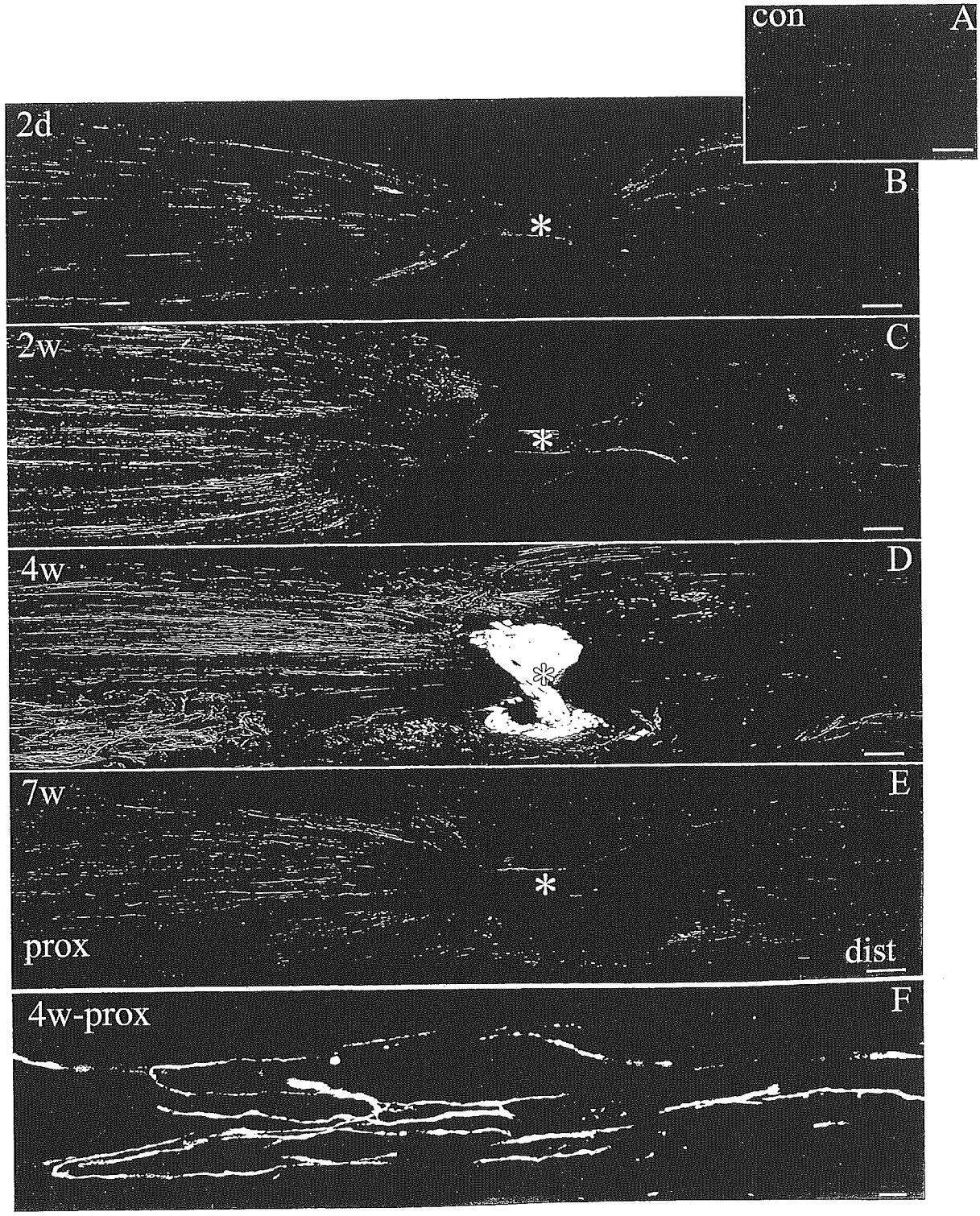

Fig. 1. Legend on the opposite page.

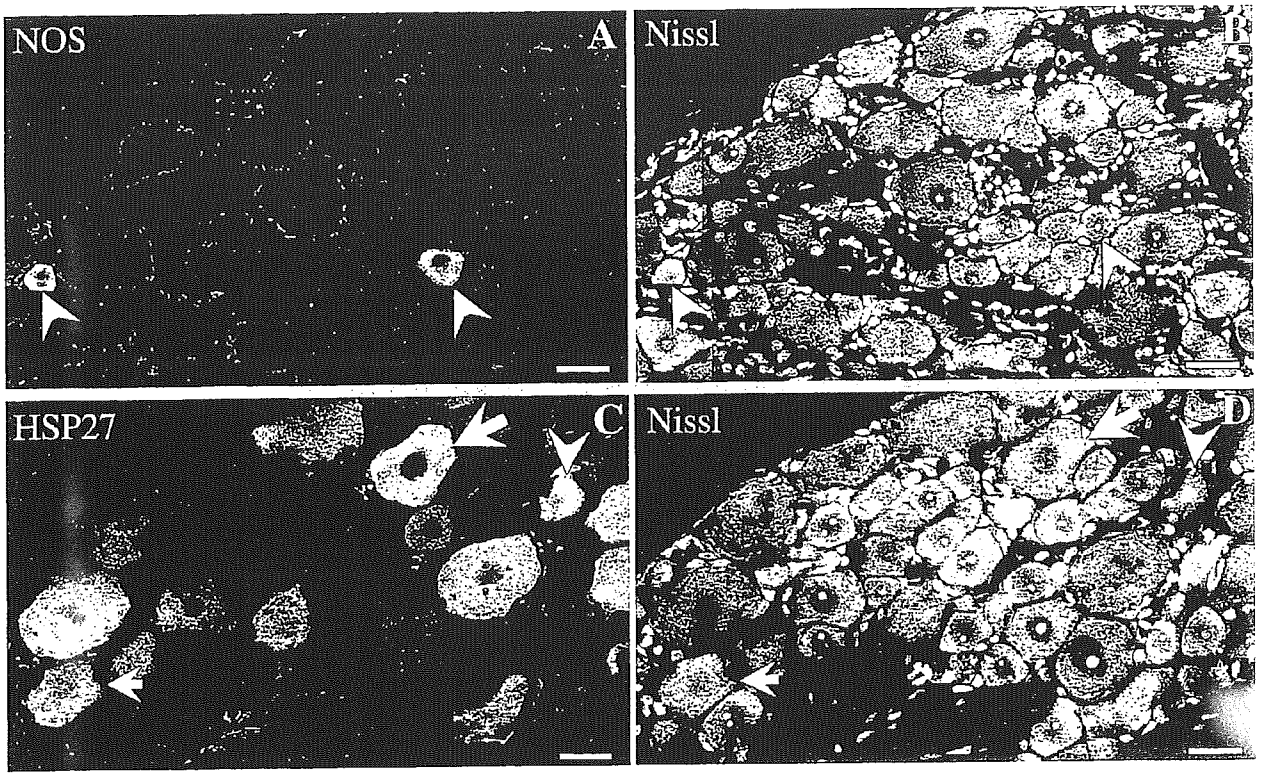

Fig. 2. A NOS immunofluorescent-labeled (**A**) and fluorescent Nissl-stained (**B**) section and an HSP27 immunofluorescent-labeled (**C**) and fluorescent Nissl-stained (**D**) section of L5 DRG from an intact animal. Arrowheads indicate small neurons, and the small or large arrow shows a medium or large neuron, respectively. Scale bars=30 μm

immunofluorescent labeling of NOS and fluorescent Nissl staining. The sciatic nerve sections were only processed for immunofluorescent labeling of NOS.

The immunohistochemical procedures used in the present study has been described in detail in our previous articles (He *et al.*, 2003; Hirata *et al.*, 2003). Briefly, non-specific binding sites were blocked by preincubation with 0.1% bovine serum albumin (BSA) in PBS containing 0.5% Triton X-100 overnight at 4℃. For single immunfluorescent labeling of NOS, the sections were first incubated with sheep polyclonal antibodies (pAb) raised against brain NOS (1:2000; donated by Dr. Emson) and then with biotinylated donkey anti-sheep IgG (Jackson, USA) overnight at room temperature (RT). For visualization of the biotin-binding site, Texas red-streptavidin was used. For single immunofluorescent labeling of HSP27, rabbit pAb raised against murine HSP25 which specifically recognized rat HSP27 (Head *et al.*, 1994; Plumier *et al.*, 1996) (StressGen, SPA-801) was used. The sections were first incubated with rabbit pAb to HSP25/27 diluted in PBS (1:1500) for 36 h at RT and then with Texas red-conjugated donkey anti-rabbit IgG (Jackson) overnight at RT. Control sections were processed in the same way and in parallel, except that they were incubated with PBS instead of primary antibodies. No stained structures were observed in the controls. The sections Texas red-labeled for NOS or HSP27 were counter-stained with green fluorescent Nissl-stain solution (NeuroTrace 500/525 green fluorescent Nissl-stain, N-21480, Molecular Probes) for quantifying the total number of DRG neurons (cf. Fig. 2A, B, C, D).

For double immunofluorescent labeling of HSP27 and NOS, a mixture of rabbit pAb to HSP25/27 and sheep pAb to NOS was used as the primary antibody. Then a mixture of Texas red-conjugated donkey anti-rabbit IgG (Jackson) and Alexa488-conjugated donkey anti-goat IgG (Molecular Probes) was used as the secondary antibody. No differences in the morphology of any of the immunolabeled structures were noted between the single and double labeled samples.

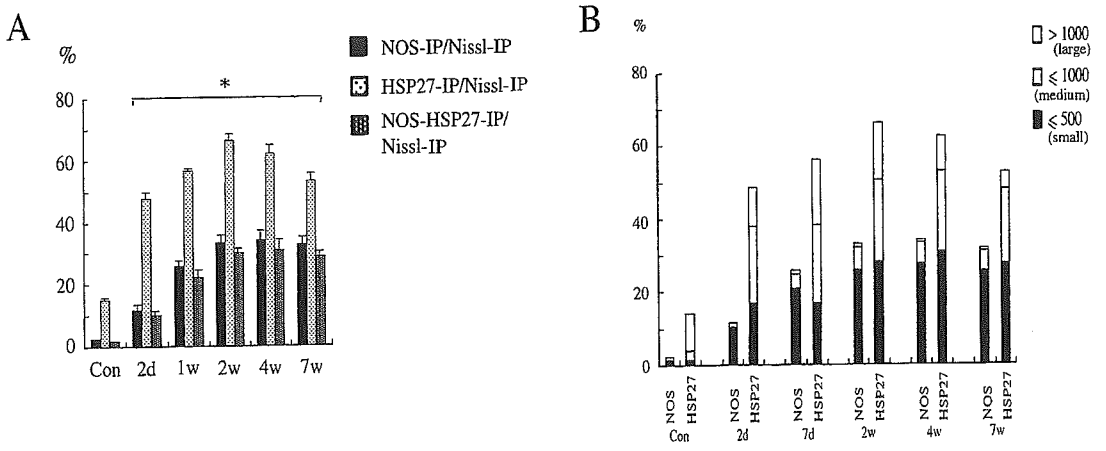

Fig. 3. A: Changes in the number of NOS-, HSP27-immunoreactive and NOS- and HSP27-double-immunoreactive neurons in the L5 DRGs following sciatic nerve ligation. Three animals were used at each time point. Data are the mean ± S.D. (bars). Values of NOS- and HSP27-immunoreactive neurons are expressed as percentages compared with the total number of fluorescent Nissl-stained DRG neurons in each of the same sections, and that of NOS- and HSP27-double-immunoreactive neurons have been compared with the average of the total number. * $p<0.05$. **B:** Changes in neuronal size in NOS- and HSP27-immunoreactive DRG neurons following sciatic nerve ligation. Three animals were used at each time point. Note that a gradual increase and subsequent persistent occurrence of NOS-immunoreactive small neurons occur after nerve ligation, paralleling the occurrence of HSP27-immunoreactive small neurons.

Retrograde tracing with a fluorescent dye

To examine whether NOS-immunoreactive small DRG neurons forming a pericellular basket were axotomized, three animals received an application of a retrograde fluorescent tracer, dextran fluorescein (FITC) (3000 MW, anionic lysine fixable, Molecular Probes) at 9 weeks after ligation. The ligated sciatic nerve was cut at a point 1 mm proximal from the ligation site, and the proximal stump was placed in 2 μl of 4% saline-dissolved dextran FITC in a small plastic tube with a blinded end. The nerve was then glue-packed in the tube to prevent any leakage of the tracer. Two or three days after tracer injection, the animals were perfused with the same fixative and the DRGs were removed (Kobayashi *et al.*, 2003). The sections were processed for NOS immunohistochemistry and labeled with Texas red.

Confocal laser scanning microscopy

The sections double-labeled with one of the green fluorescent dyes (Nissl, Alexa 488, or FITC) and Texas red were scanned using excitation at 488 nm (argon laser) for the former and at 568 nm (krypton laser) for the latter by confocal laser scanning microscopy (CLMS; LSM-GB200, Olympus, Japan). Images were scanned using a 10 × objective lens. To avoid cross-talk, separate single optical sections were scanned for each fluorescence (channels 1 and 2) and then superimposed. For the pericellular baskets, images were taken using a 40 × objective lens, and serial optical sections were projected at intervals of 1.2 μm and extended on a single plane with a thickness of 12 to 14 μm (volume projection method).

Counting of neurons and pericellular baskets

Changes in the number of the immunoreactive neurons at each time point were analyzed by using the NIH image program. In every fourth section, the total numbers of HSP27- and NOS-immunoreactive, or HSP27- and NOS-double-immunoreactive neurons with a clearly visible nucleus, were separately counted. The ratio of NOS- or HSP27-immunoreactive neurons was expressed as a percentage to the total number of fluorescent Nissl-stained DRG neurons in the same section . The ratio of NOS- and

HSP27-double-immunoreactive neurons was expressed as a percentage to the average total number of fluorescent Nissl-stained neurons in the next two sections. The total number of fluorescent Nissl-stained neurons showed no significant difference among DRGs from ipsilateral and contralateral sides, and intact animals. Two forms of Student's t-test were utilized to compare the means of each parameter. To increase the reliability of measured data, Student's t-test was applied between DRGs from the ipsilateral sides and controls. The difference between the two values was considered significant if the probability value (P) was less than 0.05.

The number of pericellular baskets was counted in NOS- and HSP27-double-immunofluorescent labeled sections and NOS-immunofluorescent labeled sections treated with retrograde labeling. A pericellular basket was defined as a NOS-immunoreactive component running closely adjacent to the somatic profile >70 % of its circumference.

Size measurements

Changes in the sizes of the NOS- or HSP27-immunoreactive DRG neurons at each time point were analyzed by tracing the circumferences of the somata using the same image program.

All experiments were reviewed by the Committee on Ethics for Animal Experiments of the Faculty of Medicine, Kyushu University, and carried out according to the University's Guidelines for Animal Experiments and Law No. 105 and Notification No. 6 of the Japanese Government.

Results

NOS immunohistochemistry in sciatic nerves

In the intact sciatic nerves, few NOS-immunoreactive fibers were seen (Fig. 1A), but at 2 days after ligation, a small number of NOS-immunoreactive fibers appeared in the proximal stump near the ligature (Fig. 1B). At 2 weeks, the proximal stump was extremely swollen and numerous NOS-immunoreactive fibers with strong immunoreactivity were seen (Fig. 1C). At 4 weeks, the increased numbers of NOS-immunoreactive fibers were still visible in the proximal stump, but some ran alongside the ligature towards the distal stump (Fig. 1D). At higher magnification, the NOS-immunoreactive fibers in the proximal stump with strong immunoreactivity showed profiles characteristic of regrowing axons, such as varicosities and swelling in the sinuous course as previously reported by Gonzalez-Hernandez and Rustioni (1999), and they often became recurrent (Cajal, 1928) (Fig. 1F). Thereafter, the NOS-immunoreactive fibers gradually decreased and only a small number with less immunoreactivity were detected at 7 weeks (Fig. 1E).

NOS and HSP27 immunohistochemistry in DRGs

In the DRGs of the contralateral side and from intact animals, NOS was weakly expressed in a small number of neurons (approximately 2%) (Fig. 2A, B, 3A, B), whereas HSP27 was expressed in a greater number (about 14%) (Fig. 2C, D, 3A, B) with varying degrees of immunoreactivity (Fig. 4A). The NOS-immunoreactive neurons consisted of small (100-500 μm^2) (Fig. 2A, B) to medium neurons (500−1000 μm^2) (Fig. 3B), whereas HSP27-immunoreactive neurons consisted of a majority of large neurons (>1000 μm^2) with a small proportion of small and medium neurons (Fig. 2C, D, 3B). Double immunofluorescent labeling showed that most of the NOS-immunoreactive neurons were positive for HSP27 (Fig. 3A) although the expression of both proteins was usually weak (Fig. 4A).

After sciatic nerve ligation, the NOS-immunoreactive neurons significantly increased in number (Fig. 3A) and usually showed strong immunoreactivity (Fig. 4B, C, D). At 2 days, NOS-immunoreactive neurons comprised six times the original number in the controls (approximately 12%), then gradually increased and reached a peak at 2 weeks (approximately 33%). Thereafter the NOS-immunoreactive neurons maintained strong immunoreactivity until 7 weeks (Fig. 3A) even though the NOS-immunoreactive fibers within the sciatic nerves decreased at this point (Fig. 1E). Size frequency analysis (Fig. 3B) revealed that the majority of *de novo* NOS-immunoreactive subpopulations at each

Fig. 4. Pseudo-color images of the double immunofluorescent labeling of NOS (green) and HSP27 (red) in the DRG from an intact animal (**A**) and ipsilateral DRGs at 2 days (**B**), 2 weeks (**C**) and 7 weeks (**D**) after sciatic nerve ligation. Only one weakly stained NOS and HSP27-double-immunoreactive small neuron (yellowish green) is seen in the intact DRG (**A**). Intensely stained NOS and HSP27-double-immunoreactive small neurons (bright yellow) appear at 2 days (**B**) and increase at 2 weeks (**C**) after ligation. At 7 weeks (**D**), HSP27 expression becomes weaker in most double-immunoreactive small neurons so that most become yellowish green. Scale bar= 100 μm (for A−D)

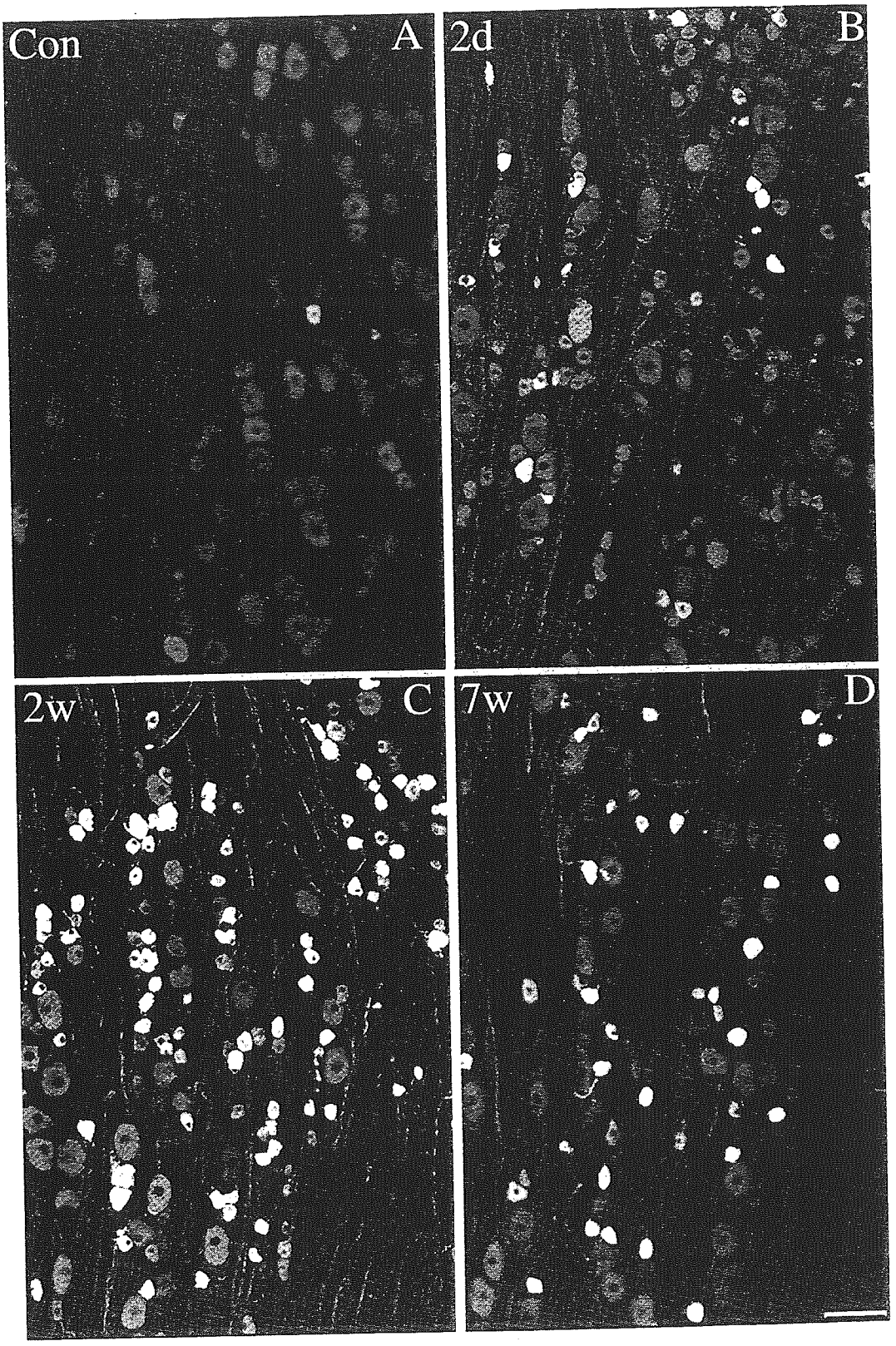

Fig. 4. Legend on the opposite page.

time point after ligation were composed of small neurons.

After nerve ligation, the HSP27-immunoreactive neurons also increased in number (Fig. 3A) and some of them, especially the small neurons, showed stronger immunoreactivity (Fig. 4B, C) than that seen in the controls. At 2 days, HSP27-immunoreactive neurons reached more than three times the original number in the controls (about 48%). This number further increased and reached a peak at 2 weeks (approximately 66%). They then slightly declined, reaching about 53% at 7 weeks (Fig. 3A), with most also reduced in immunoreactivity (Fig. 4D). Thus, the pattern of changes was similar between NOS- and HSP27-immunoreactive neurons until postoperative week 2, but thereafter the latter slightly decreased in number and immunoreactivity while the former remained unchanged. Size frequency analysis (Fig. 3B) showed that, after nerve ligation, the number of HSP27-immunoreactive small and medium neurons markedly increased, whereas that of HSP27-immunoreactive large neurons was only slightly altered. Especially the HSP27-immunoreactive small neurons prominently increased at 2 weeks, representing almost half of all the HSP27-immunoreactive neurons, and then remained unchanged until 7 weeks (Fig. 3B). Double immunofluorescent labeling showed that most NOS-immunoreactive neurons were also positive for HSP27 at each time point (about 87%) (Fig. 3A, 4B, C, D)—although in these neurons the HSP27 immunoreactivity was considerably reduced at 7 weeks (Fig. 4D).

Pericellular baskets formed by NOS-immunoreactive sprouts in DRGs

Observations under higher magnification revealed the formation of basket-like structures after nerve ligation, in which NOS-immunoreactive fibers usually surrounded the cell body of NOS-negative large neurons (Fig. 5A, B, D), and in some cases, that of NOS-immunoreactive small neurons (Fig. 5C). This pericellular basket was hardly visible at 2 weeks although at this time point NOS-immunoreactive fibers appeared in the nerve bundles within the DRGs (Fig. 4C), occurring concurrently with the marked increase in the proximal stump of the sciatic nerves (Fig. 1C). The NOS-immunoreactive baskets were first detected at 5 weeks and thereafter the numbers increased. We counted the number of baskets in every second section at 7 and 9 weeks. At 7 weeks after nerve ligation, the density of NOS-immunoreactive baskets ranged from 0.4 to 3.2/section in the L5 DRG of 3 rats (mean 1.4 ± 0.5, n=30 sections). At 9 weeks, it ranged from 2.4 to 3.2/section among 3 rats (mean 2.8 ± 1.3, n=38 sections). These findings suggest that the formation of the baskets was ongoing during this period. Double immunofluorescent labeling showed that the NOS-immunoreactive baskets hardly coexpressed with HSP27 (Fig. 5A). No pericellular baskets were detected in DRG sections from intact animals (n=16 sections), and only 2 were seen in a few sections from the contralateral side (n=12 sections). Thus, most of the baskets seemed to appear as a direct result of peripheral nerve ligation. In some cases the NOS-immunoreactive fibers that formed the baskets could be traced to their origin and were shown to be formed by axonal sprouts from cell bodies of NOS-immunoreactive small neurons lying 1–3 cell diameters away (Fig. 5B, D).

NOS-immunohistochemistry of the DRG receiving a retrograde labeling with a fluorescent tracer, dextran-FITC, revealed that most of the NOS-immunoreactive small neurons became heavily retrograde-labeled (Fig. 5D). NOS negative large neurons surrounded by the NOS-immunoreactive baskets were also often labeled with dextran-FITC although they were usually less intensely labeled compared with small neurons (Fig. 5D). Retrograde labeling was detected in about 82% (82/99) of the neurons associated with NOS-immunoreactive baskets. Consequently, in some cases the axonal sprout from the dextran-labeled NOS-immunoreactive neurons formed the baskets around the dextran-labeled NOS negative large neurons (Fig. 5D). Thus, these findings suggest the possibility of a rewiring of two classes of axotomized neurons.

Discussion

The present study has clearly shown a significant increase in NOS-immunoreactive DRG neurons after sciatic nerve ligation. This result is basically in accordance with that studied in various experimental models of peripheral nerve injury, such as transection (Fiallos-Estrada *et al.*, 1993; Zhang *et al.*, 1993), resection (Verge *et al.*, 1992; Thippeswamy *et al.*, 2001), loose ligation (Cizkova *et al.*, 2002) and tight ligation (Gonzalez-Hernandez and Rustioni, 1999) of the sciatic nerves, and tight ligation of L5 and L6 spinal nerves (Luo *et al.*, 1999). The increased NOS-immunoreactive DRG neurons were mainly small neurons, as reported in other studies (Gonzalez-Hernandez and Rustioni, 1999; Luo *et al.*, 1999). The number of HSP27-immunoreactive DRG neurons also increased after nerve ligation; these neurons were mainly small and medium sized, as reported Costigan *et al.* (1998).

The present study includes a new finding that the NOS-immunoreactive small neurons were mostly coexpressed with HSP27. Statistical analysis showed that the NOS and HSP27-double-immunoreactive small DRG neurons—

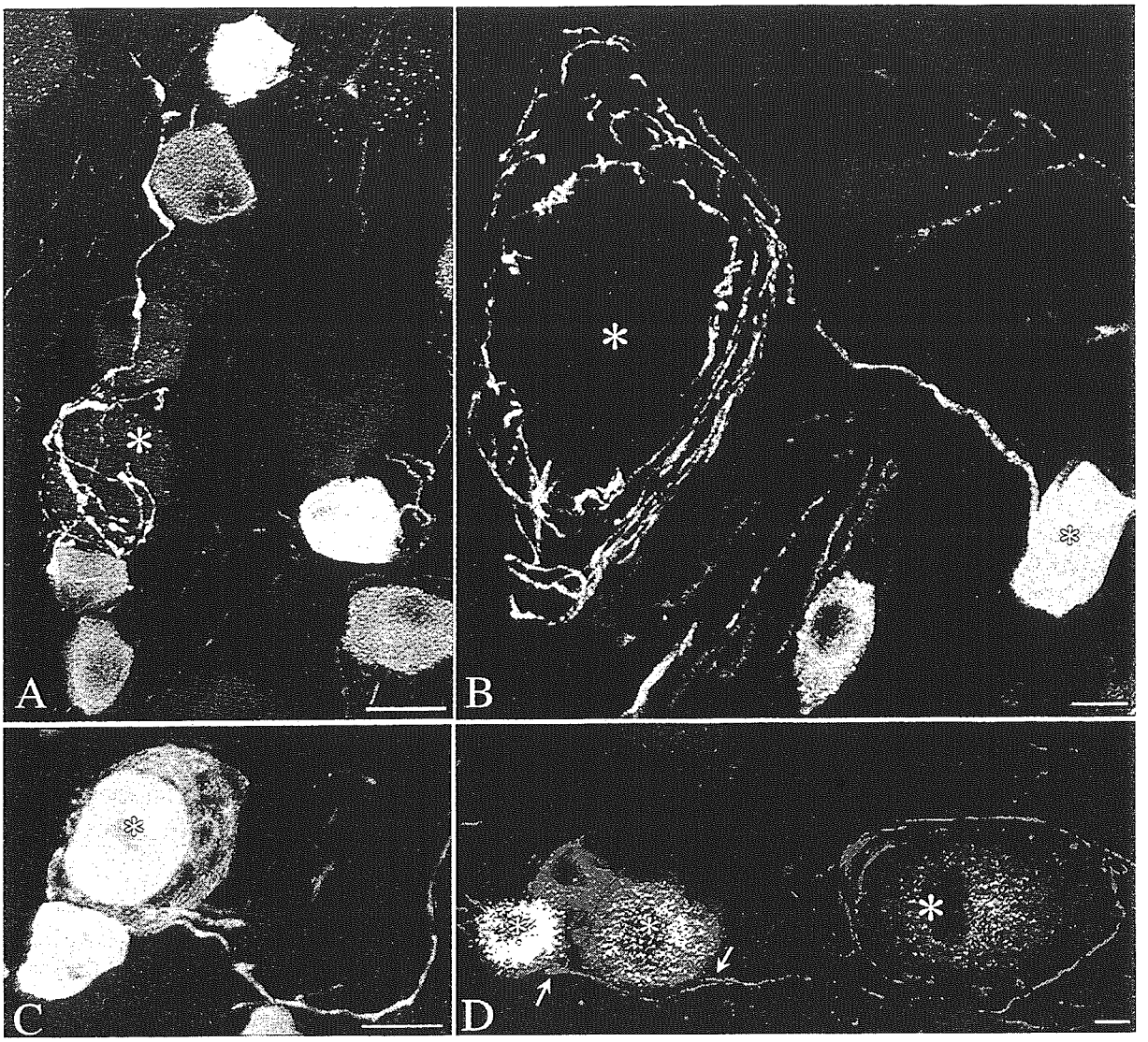

Fig. 5. Pseudo-color images of the NOS-immunoreactive baskets that form around the NOS-negative large neurons (**A**, **B** and **D**) or NOS-immunoreactive small neurons (**C**) from 5 (**A**) and 9 weeks (**B**, **C** and **D**) after sciatic nerve ligation. **A:** Double immunofluorescent labeling of NOS (green) and HSP27 (red) showing a basket consisting of an elaborate NOS-immunoreactive axonal plexus with numerous varicosities surrounding a tangentially sectioned large neuronal profile (the large asterisk). Note that no coexpression with HSP27 in the basket is seen. **B:** NOS immunofluorescent labeling showing a NOS-immunoreactive axonal sprout from a strongly stained NOS-immunoreactive small neuron (the small asterisk) repetitively surrounding a large neuronal profile (a large asterisk) presumably sectioned through the center of the neuron. **C:** NOS immunofluorescent labeling showing a smooth NOS-immunoreactive fiber repetitively surrounding an intensely stained-NOS-immunoreactive small neuron. **D:** Retrograde labeling with FITC-dextran (green or yellow) and NOS immunofluorescent labeling (red) showing that two retrograde-labeled NOS-immunoreactive small neurons (small asterisks) send axonal sprouts (arrows) to form the baskets surrounding a retrograde-labeled NOS negative large neuron (the large asterisk). Scale bars=20 μm (A–C), 10 μm (D)

the new subpopulation that occurred after axonal injury—gradually increased, reaching a maximum at 2 weeks, and then remained unchanged until postoperative week 7 although the immunoreactivity of HSP27 appeared to decrease at 7 weeks. Thus, we consider that axonal injury induced the simultaneous upregulation of the two proteins in small neurons. On the other hand, Gonzalez-Hernandez and Rustioni (1999) used the same model as presented here to show that NOS-immunoreactive neurons were coexpressed with growth-associated phosphoprotein 43 (GAP-43), and this coexpression was also seen in the regenerating axons in the sciatic nerve. They concluded that NO might contribute to the growth and regeneration of injured axons. In our study, NOS-immunoreactive fibers showing regenerating profiles appeared at 2–4 weeks when the NOS-immunoreactive neurons were maximum both in number and immunoreactivity; this might support the conclusion drawn by the previous authors. Thus, we suppose that both proteins examined in our study, NOS and HSP27, might play a neuroprotective role in small DRG neurons. The coexpression of these proteins in small neurons might also indicate that axonal damage causes a more protective neuronal response in small neurons than other larger-sized subpopulations.

The present study also demonstrated that the maximal level of NOS-immunoreactive neurons was maintained until 7 weeks after nerve injury. This finding is consistent with a previous study using sciatic nerve transection models (Fiallos-Estrada *et al.*, 1993), in which the considerable increase in NOS-immunoreactive DRG neurons persisted even until 21 weeks after transection. The lengthy expression of NOS in the small DRG neurons may be explained by the occurrence of the NOS-immunoreactive baskets surrounding NOS negative large neurons since they were formed by axonal sprouts from NOS-immunoreactive small neurons and appeared after depletion of the NOS-immunoreactive regenerating fibers in the sciatic nerve.

It has not been previously described how the NOS-containing pericellular baskets appear in the DRG after peripheral axotomy although a few studies using other neuronal markers reported the occurrence of similar structures. McLachlan *et al.* (1993) first showed that noradrenergic perivascular axons sprout in the DRGs and form basket-like structures around axotomized large DRG neurons. They thought that these unusual connections, along with the sprouting of Aβ axons terminating deep in the dorsal horn into Lamina II (Woolf *et al.*, 1992), contribute to the changes in sensory processing that might lead to neuropathic pain. Further studies demonstrated that the similar pericellular baskets were also formed by axonal sprouts of calcitonin gene-related peptide and substance P-positive small DRG neurons (McLachlan and Hu, 1998) and Isolectin B4-positive small DRG neurons(Li and Zhou, 2001), preferentially around large neurons after peripheral axotomy.

The mechanism for the formation of the pericellular baskets remains obscure. Li and Zhou (2001) assumed that changes in the neurotrophic environment encountered by small and large injured sensory neurons might lead to a rewiring of these neurons in the DRGs and spinal cord. We consider that the formation of NOS-immunoreactive pericellular baskets might be performed by a similar mechanism since trophic factors such as NGF are reported involved in the induction of NOS in small neurons (for review see Thippeswamy and Morris, 2002).

As one of the functions of induced NOS after peripheral nerve injury, it has been proposed that NO might play a role in nociceptive transmission in chronic neuropathic pain (Meller *et al.*, 1992; Choi *et al.*, 1996; Cizkova *et al.*, 2002) although Luo *et al.* (1999) cast doubt on this assumption. Retrograde labeling confirmed that both the small neurons sending the NOS-immunoreactive axonal sprout that formed the pericellular basket and the large neurons surrounded by it were axotomized. Thus, our study is first to reveal that peripheral axotomy induces abnormal connections between NOS-immunoreactive small neurons and NOS negative large neurons, suggesting the involvement of NO in rewiring these two classes of primary sensory neurons. However, further studies are needed to clarify whether NO is associated with the development of neuropathic pain.

Acknowledgements

We thank Mr. Takaaki Kanemaru (Morphology Core, Graduate School of Medical Sciences, Kyushu University) and Mr. Yasuhiro Hirakawa for their help in preparing photomicrographs, and Mr. Naoya Inakura for his expert technical assistance.

References

Bredt DS, Snyder SH: Isolation of nitric oxide synthetase, a calmodulin-requiring enzyme. *Proc Natl Acad Sci USA* 87: 682-685 (1990).

Cajal YR: *Degeneration and regeneration of the nervous system* (May RM, ed), Vol. 1. Hafner Publishing Co., NY, 1959 (p. 290-304).

Choi Y, Raja SN, Moore LC, Tobin JR: Neuropathic pain in rats is associated with altered nitric oxide synthase activity in neural tissue. *J Neurol Sci* 138: 14-20 (1996).

Ciocca DR. Oesterreich S. Chamness GC. McGuire WL. Fuqua SA: Biological and clinical implications of heat shock protein 27,000 (Hsp27): a review. *J Natl Cancer Inst* 85: 1558-1570 (1993).

Cizkova D, Lukacova N, Marsala M, Marsala J: Neuropathic pain is associated with alterations of nitric oxide synthase immunoreactivity and catalytic activity in dorsal root ganglia and spinal dorsal horn. *Brain Res Bull* 58: 161-171 (2002).

Costigan M, Mannion RJ, Kendall G, Lewis SE, Campagna JA, Coggeshall RE, Meridith-Middleton J, Tate S, Woolf CJ: Heat shock protein 27: developmental regulation and expression after peripheral nerve injury. *J Neurosci* 18: 5891-5900 (1998).

Estevez AG, Spear N, Manuel SM, Radi R, Hendersin CE, Barbeito L, Beckman JS: Nitric oxide and superoxide contribute to motor neuron apoptosis induced by trophic factor deprivation. *J Neurosci* 18: 923-931 (1998).

Fiallos-Estrada CE, Kummer W, Mayer B, Bravo R, Zimmermann M, Herdegen T: Long-lasting increase of nitric oxide synthase immunoreactivity, NADPH-diaphorase reaction and c-JUN co-expression in rat dorsal root ganglion neurons following sciatic nerve transection. *Neurosci Lett* 150: 169-173 (1993).

Gonzalez-Hernandez T, Rustioni A: Nitric oxide synthase and growth-associated protein are coexpressed in primary sensory neurons after peripheral injury. *J Comp Neurol* 404: 64-74 (1999).

He J, Hirata K, Wang S, Kawabuchi M: Expression of nitric oxide synthase and 27-kD heat shock proteins in motor neurons of ventral root-avulsed rats. *Arch Histol Cytol* 66: 83-93 (2003).

Head MW, Corbin E, Goldman JE: Coordinate and independent regulation of alpha B-crystallin and hsp27 expression in response to physiological stress. *J Cell Physiol* 159: 41-50 (1994).

Hirata K, He J, Hirakawa Y, Liu W, Wang S, Kawabuchi M: HSP27 is markedly induced in Schwann cell columns and the associated regenerating axons. *Glia* 42: 1-11 (2003).

Iadicola C: Bright and dark sides of nitric oxide in ischemic brain injury. *Trends Neurosci* 20: 132-139 (1997).

Imura T, Shimohama S, Sato M, Nishikawa H, Madono K, Akaike A, Kimura J: Differential expression of small heat shock proteins in reactive astrocytes after focal ischemia: possible role of beta-adrenergic receptor. *J Neurosci* 19: 9768-9779 (1999).

Iwaki T, Iwaki A, Tateishi J, Sakaki Y, Goldman JE: Alpha B-crystallin and 27-kd heat shock protein are regulated by stress conditions in the central nervous system and accumulate in Rosenthal fibers. *Amer J Pathol* 143: 487-495 (1993).

Kato H, Liu Y, Kogure K, Kato K: Induction of 27-kDa heat shock protein following cerebral ischemia in a rat model of ischemic tolerance. *Brain Res* 634: 235-244 (1994).

Kato H, Kogure K, Liu XH, Araki T, Kato K, Itoyama Y: Immunohistochemical localization of the low molecular weight stress protein HSP27 following focal cerebral ischemia in the rat. *Brain Res* 679: 1-7 (1995).

Kobayashi S, Koyama J, Yokouchi K, Fukushima N, Oikawa S, Moriizumi T: Functionally essential neuronal population of the facial motor nucleus. *Neurosci Res* 45:357-361 (2003).

Krumenacker JS, Hanafy KA, Murad F: Regulation of nitric oxide and soluble guanylyl cyclase. *Brain Res Bull* 62: 505-515 (2004).

Lewis SE, Mannion RJ, White FA, Coggeshall RE, Beggs S, Costigan M, Martin JL, Dillmann WH, Woolf CJ: A role for HSP27 in sensory neuron survival. *J Neurosci* 19: 8945-8953 (1999).

Li L, Zhou XF: Pericellular Griffonia simplicifolia I isolectin B4-binding ring structures in the dorsal root ganglia following peripheral nerve injury in rats. *J Comp Neurol* 439: 259-274 (2001).

Luo ZD, Chaplan SR, Scott BP, Cizkova D, Calcutt NA, Yaksh TL: Neuronal nitric oxide synthase mRNA upregulation in rat sensory neurons after spinal nerve ligation: lack of a role in allodynia development. *J Neurosci* 19: 9201-9208 (1999).

McLachlan EM, Hu P: Axonal sprouts containing calcionin gene-related peptide and substance P form pericellular baskets around large diameter neurons after sciatic nerve transection in the rat. *Neuroscience* 84: 961-965 (1998).

McLachlan EM, Janig W, Devor M, Mivhaelis M: Peripheral nerve injury triggers noradrenergic sprouting within dorsal root ganglia. *Nature* 363: 543-546 (1993).

Meller ST, Pechmans PS, Gebhart GF, Maves TJ: Nitric oxide mediates the thermal hyperalgesia prodeced in a model of neuropathic pain in the rat. *Neuroscience* 50: 7-10 (1992).

Novikov L, Novikova L, Kellerth JO: Brain-derived neurotrophic factor promotes survival and blocks nitric oxide synthase expression in adult rat spinal motoneurons after ventral root avulsion. *Neurosci Lett* 200: 45-48 (1995).

Plumier JC, Armstrong JN, Landry J, Babity JM, Robertson HA, Currie RW: Expression of the 27,000 mol. wt heat shock protein following kainic acid-induced status epilepticus in the rat. *Neuroscience* 75: 849-856 (1996).

Renkawek K, Bosman GJ, de Jong WW: Expression of small heat-shock protein hsp 27 in reactive gliosis in Alzheimer disease and other types of dementia. *Acta Neuropathol (Berl)* 87: 155-160 (1994).

Shinohara H, Inaguma Y, Goto S, Inagaki T, Kato K: Alpha B crystallin and HSP28 are enhanced in the cerebral cortex of patients with Alzheimer's disease. *J Neurol Sci* 119: 203-208 (1993).

Thippeswamy T, Morris R: The roles of nitric oxide in dorsal root ganglion neurons. *Ann NY Acad Sci* 962: 103-110 (2002).

Thippeswamy T, Jain RK, Mumtaz N, Morris R: Inhibition of neuronal nitric oxide synthase results in neurodegeneration changes in the axotomised dorsal root ganglion neurons: evidence for a neuroprotective role of nitric oxide in vivo. *Neurosci Res* 40: 37-44 (2001).

Verge VM, Xu Z, Xu XJ, Wiesenfeld-Hallin Z, Hokfelt T: Marked increase in nitric oxide synthase mRNA in rat dorsal root ganglia after peripheral axotomy: in situ hybridization and functional studies. *Proc Natl Acad Sci USA* 89: 11617-11621 (1992).

Woolf CJ, Shortland P, Coggeshall RE: Peripheral nerve injury triggers central sprouting of myelinated afferents. *Nature* 355: 75-78 (1992).

Wu W, Li L: Inhibition of nitric oxide synthase reduces motoneuron death due to spinal root avulsion. *Neurosci Lett* 153: 121-124 (1993).

Wu W, Han K, Li L, Schinco FP: Implantation of PNS graft inhibits the induction of neuronal nitric oxide synthase and enhances the survival of spinal motoneurons following root avulsion. *Exp Neurol* 129: 335-339 (1994).

Zhang X, Verge V, Wiesenfeld-Hallin Z, Ju G, Bredt D, Synder SH, Hokfelt T: Nitric oxide synthase-like immunoreactivity in lumbar dorsal root ganglia and spinal cord of rat and monkey and effect of peripheral axotomy. *J Comp Neurol* 22: 563-575 (1993).

doi:10.1093/brain/awh453 *Brain* (2005), **128**, 988–1002

Intrathecal activation of the IL-17/IL-8 axis in opticospinal multiple sclerosis

Takaaki Ishizu,[1] Manabu Osoegawa,[1] Feng-Jun Mei,[1] Hitoshi Kikuchi,[1] Masahito Tanaka,[1] Yuka Takakura,[1] Motozumi Minohara,[1] Hiroyuki Murai,[1] Futoshi Mihara,[2] Takayuki Taniwaki[1] and Jun-ichi Kira[1]

[1]*Department of Neurology, Neurological Institute and* [2]*Division of Neuroradiology, Department of Radiology, Graduate School of Medical Sciences, Kyushu University, Fukuoka, Japan*

Correspondence to: Professor J. Kira, Department of Neurology, Neurological Institute, Graduate School of Medical Sciences, Kyushu University, 3-1-1 Maidashi, Higashiku, Fukuoka 812-8582, Japan
E-mail: kira@neuro.med.kyushu-u.ac.jp

Summary

There are two distinct subtypes of multiple sclerosis in Asians, opticospinal (OS-multiple sclerosis) and conventional (C-multiple sclerosis). In OS-multiple sclerosis, selective and severe involvement of the optic nerves and spinal cord is characteristic, though its mechanisms are unknown. The present study aimed to find out possible differences in the cytokine/chemokine profiles in CSF between OS-multiple sclerosis and C-multiple sclerosis and to delineate the relationships between these profiles and neuroimaging and pathological features. Sixteen cytokines/chemokines, namely interleukin (IL)-1β, IL-2, IL-4, IL-5, IL-6, IL-7, IL-8, IL-10, IL-12 (p70), IL-13, IL-17, interferon (IFN)-γ, tumour necrosis factor (TNF)-α, granulocyte colony-stimulating factor (G-CSF), monocyte chemoattractant protein-1 (MCP-1) and macrophage inflammatory protein-1β (MIP-1β), were measured simultaneously in CSF supernatants from 40 patients with relapsing–remitting multiple sclerosis (20 OS-multiple sclerosis and 20 C-multiple sclerosis) at relapse and 19 control patients with spinocerebellar degeneration (SCD), together with intracellular production of IFN-γ and IL-4 in CSF $CD4^+$ T cells. In CSF supernatants relative to controls, IL-17, MIP-1β, IL-1β and IL-13 were only significantly increased in OS-multiple sclerosis patients, while TNF-α was only significantly increased in C-multiple sclerosis patients, using a cut-off level of 1 pg/ml. IL-8 was significantly elevated in both OS-multiple sclerosis and C-multiple sclerosis patients. MCP-1 was significantly decreased in both OS-multiple sclerosis and C-multiple sclerosis patients, while IL-7 was only significantly decreased in C-multiple sclerosis patients. IL-17, IL-8 and IL-5 were significantly higher in OS-multiple sclerosis patients than in C-multiple sclerosis patients. The increases in IL-17 and IL-8 in OS-multiple sclerosis were still significant even after exclusion of the patients undergoing various immunomodulatory therapies. Assays of intracellular cytokine production revealed that both the IFN-γ^+IL-4^- T-cell percentage and intracellular IFN-γ/IL-4 ratio in CSF cells were significantly greater in C-multiple sclerosis patients than in controls. Contrarily, OS-multiple sclerosis patients showed not only a significantly greater percentage of IFN-γ^+IL-4^- T cells than controls but also a significantly higher percentage of IFN-γ^-IL-4^+ T cells than C-multiple sclerosis patients. Among the cytokines elevated in multiple sclerosis, only IL-8 showed a significant positive correlation with the Expanded Disability Status Scale of Kurtzke score. Both the length of the spinal cord lesions on MRI and the CSF/serum albumin ratio had a significant positive correlation with IL-8 and IL-17 in multiple sclerosis, in which the spinal cord lesions were significantly longer in OS-multiple sclerosis than in C-multiple sclerosis. Three of six spinal cord specimens from autopsied OS-multiple sclerosis cases demonstrated numerous myeloperoxidase-positive neutrophils infiltrating necrotic lesions. These findings strongly suggest that in OS-multiple sclerosis, in addition to the Th1 cell upregulation seen in C-multiple sclerosis, intrathecal activation of the IL-17/IL-8 axis inducing heavy neutrophil infiltration contributes to extensive spinal cord lesion formation.

Keywords: multiple sclerosis; cytokine; chemokine; cerebrospinal fluid; neutrophil

Abbreviations: C-multiple sclerosis = conventional form of multiple sclerosis; EAE = experimental allergic encephalomyelitis; EDSS = Expanded Disability Status Scale of Kurtzke; G-CSF = granulocyte colony-stimulating factor; IFN = interferon; IL = interleukin; LP = lumbar puncture; MCP-1 = monocyte chemoattractant protein-1; MIP-1β = macrophage

inflammatory protein-1β; NMO = neuromyelitis optica; OS-multiple sclerosis = opticospinal form of multiple sclerosis; PBL = peripheral blood lymphocyte; SCD = spinocerebellar degeneration; TNF = tumour necrosis factor

Received September 20, 2004. Revised October 24, 2004. Accepted January 26, 2005. Advance Access publication March 2, 2005

Introduction

Multiple sclerosis is a chronic inflammatory disease of the CNS characterized by macrophage and lymphocyte infiltration, demyelination, axonal injury and loss of neurological function. It has been hypothesized, but not yet proven, to be caused by an autoimmune mechanism targeting CNS myelin.

Cytokines are soluble proteins that mediate and regulate interactions between cells of the immune system, and are key mediators of autoimmune attack against CNS myelin (Huang *et al.*, 1999). In multiple sclerosis, many prior studies have documented that proinflammatory (Th1 type) cytokines such as interferon (IFN)-γ, tumour necrosis factor (TNF)-α, interleukin (IL)-1, IL-2 and IL-12 (p40) are involved in the onset and perpetuation of the disease, while, in contrast, anti-inflammatory (Th2 type) cytokines such as IL-4, IL-10 and transforming growth factor-β are downregulated during phases of disease activity and upregulated in phases of disease remission (Panitch *et al.*, 1987; Sharief and Hentges, 1991; Sharief and Thompson, 1993; Link *et al.*, 1994; Rieckmann *et al.*, 1994; Matusevicius *et al.*, 1996; Navikas and Link, 1996; Navikas *et al.*, 1996; Monteyne *et al.*, 1997; Fassbender *et al.*, 1998; Link, 1998; Huang *et al.*, 1999; van Boxel-Dezaire *et al.*, 1999).

It has been hypothesized that the progression of multiple sclerosis, and perhaps even its induction, may be causally related to dysregulation of the balance between Th1 and Th2 cytokines (Olsson, 1995). However, other reports have suggested that the Th1/Th2 cytokine paradigm for multiple sclerosis is an oversimplification, and that various other immune cells, including Th2, $CD8^+$ T and B cells, are involved in the complex and heterogeneous mechanisms in this condition (Laman *et al.*, 1998; Hemmer *et al.*, 2002; Lassmann and Ransohoff, 2004). Multiple cytokines often function as complexes, with the function of one inducing the function of another in a cascade effect. In this regard, multiplexed fluorescent bead-based immunoassays, which have a dynamic range of standard curves and require only small amounts of material for simultaneous measurements of numerous cytokines and chemokines, are more useful than enzyme-linked immunosorbent assay (ELISA) methods (Vignali, 2000; Kellar *et al.*, 2001; de Jager *et al.*, 2003).

Multiple sclerosis is rare in Asians but, when it does appear, the destruction of the optic nerves and spinal cord is striking (Kira, 2003). We previously reported the existence of two subtypes of multiple sclerosis in Japanese, the opticospinal form (OS-multiple sclerosis) that shows selective and severe involvement of the optic nerves and spinal cord, and the conventional form (C-multiple sclerosis) that shows disseminated lesions in the CNS including the cerebrum, cerebellum and brainstem (Kira *et al.*, 1996). The two subtypes have different clinical and neuroimaging features, and immunogenetic backgrounds (Kira *et al.*, 1996; Yamasaki *et al.*, 1999; Kira, 2003). OS-multiple sclerosis has distinct features, such as a higher age at onset, marked female preponderance and a higher Kurtzke's Expanded Disability Status Scale (EDSS) score (Kurtzke, 1983), resulting from severe visual impairment and marked spinal cord dysfunction compared with C-multiple sclerosis. Severe inflammatory destruction has been suggested in OS-multiple sclerosis, because of the occasionally higher cell counts and protein amounts in the CSF, as well as long swollen lesions extending over several vertebral segments on spinal cord MRI (Kira, 2003). Furthermore, pathological studies have revealed not only demyelination, but also axonal loss, necrosis, cavity formation, thickened vessel wall and capillary proliferation in OS-multiple sclerosis lesions (Shiraki, 1965; Ikuta *et al.*, 1982; Tabira and Tateishi, 1982). These clinico-pathological features of OS-multiple sclerosis in Asians are similar to those of a relapsing–remitting form of Devic's neuromyelitis optica (NMO) in a Western population (Wingerchuk *et al.*, 1999; Cree *et al.*, 2002; Lucchinetti *et al.*, 2002). Considerable overlap and common mechanisms between the two conditions are supposed, as seen in the recent discovery of NMO-IgG, commonly found in both (Lennon *et al.*, 2004); however, the immune mechanisms responsible for such distinct clinico-pathological features remain unknown.

Although many studies have been published on cytokine/chemokine alterations in multiple sclerosis, subtype-related alterations have been poorly characterized. We previously reported that OS-multiple sclerosis showed a significant Th1/Tc1 shift through relapse and remission phases in peripheral blood lymphocytes (PBLs), while C-multiple sclerosis only showed a significant Th1 shift during a relapse phase (Horiuchi *et al.*, 2000; Wu *et al.*, 2000; Ochi *et al.*, 2001). In CSF, except for one report disclosing a greater increase in macrophage migration inhibitory factor (MIF) in OS-multiple sclerosis than in C-multiple sclerosis (Niino *et al.*, 2000), OS-multiple sclerosis-related changes in CSF cytokine/chemokine profiles have not been investigated, probably because of the low concentrations of cytokines/chemokines and the fragility and limited numbers of CSF cells.

Therefore, in the present study, we attempted to uncover OS-multiple sclerosis-related cytokine/chemokine alterations in CSF that could explain the distinct neuroimaging and pathological features. First, we simultaneously measured 16 cytokines/chemokines, namely IL-1β, IL-2, IL-4, IL-5, IL-6, IL-7, IL-8, IL-10, IL-12 (p70), IL-13, IL-17, IFN-γ, TNF-α, granulocyte colony-stimulating factor (G-CSF),

Table 1 *Demographic features of OS-multiple sclerosis and C-multiple sclerosis patients*

	CSF supernatants assays		Intracellular cytokine production assays	
	OS-multiple sclerosis	C-multiple sclerosis	OS-multiple sclerosis	C-multiple sclerosis
No. of patients	20	20	11	13
Sex (F/M)	19/1	16/4	11/0	11/2
Age at onset (years)	44.2 ± 16.9*	25.8 ± 8.9	48.5 ± 21.8*	30.2 ± 15.2
Age at LP (years)	51.0 ± 15.1*	31.6 ± 9.6	54.6 ± 18.3*	37.2 ± 14.3
Duration of disease (years)	6.3 ± 5.4	6.1 ± 7.1	6.1 ± 5.0	7.2 ± 8.3
No. of relapses	7.3 ± 5.1	6.1 ± 5.7	5.7 ± 4.0	5.9 ± 6.0
EDSS	5.5 ± 2.3*	4.0 ± 1.8	5.0 ± 2.2	4.4 ± 1.8
CSF				
Cell count (/μl)	3.6 ± 8.0	4.2 ± 6.8	0.8 ± 1.2	1.8 ± 1.7
Total protein (mg/dl)	43.0 ± 22.5	37.7 ± 23.8	37.4 ± 15.2	39.6 ± 18.3
CSF/serum albumin ratio (10^{-4})	90.0 ± 44.0*	58.0 ± 41.2	91.5 ± 41.4*	52.0 ± 24.1
IgG index	0.674 ± 0.179	0.837 ± 0.414	0.843 ± 0.694	0.853 ± 0.306

Values are expressed as the mean ± SD. The CSF cell count and total protein amount in the control patients used for the CSF supernatant assays were 0.6 ± 0.6/μl and 28.6 ± 9.5 mg/dl, respectively, while those used for the intracellular cytokine production assays were 0.8 ± 1.1/μl and 33.5 ± 9.6 mg/dl, respectively. The numbers of patients whose CSF/serum albumin ratio and IgG index were measured were 14 in OS-multiple sclerosis and 16 in C-multiple sclerosis in the supernatants assays and eight in OS-multiple sclerosis and eight in C-multiple sclerosis in the intracellular cytokine production assays. OS-multiple sclerosis = opticospinal form of multiple sclerosis; C-multiple sclerosis = conventional form of multiple sclerosis; LP = lumbar puncture; EDSS = Expanded Disability Status Scale of Kurtzke.
*$P < 0.05$.

monocyte chemoattractant protein 1 (MCP-1) and macrophage inflammatory protein 1β (MIP-1β), in the CSF from OS-multiple sclerosis and C-multiple sclerosis patients at relapse using a multiplexed fluorescent bead-based immunoassay. Secondly, we examined the intracellular production of IFN-γ and IL-4 in CSF $CD4^+$ T cells from OS-multiple sclerosis and C-multiple sclerosis patients by flow cytometry. Thirdly, we analysed relationships among CSF cytokine/chemokine changes and clinical and spinal cord MRI findings, as well as neuropathological findings for autopsied spinal cord specimens from multiple sclerosis patients.

Materials and methods

Patients

Cytokine and chemokine assays of CSF supernatants were performed using CSF from multiple sclerosis patients exclusively at the time of clinical relapse (within 30 days of the onset of acute or subacute exacerbation). For these assays, 40 patients with relapsing–remitting multiple sclerosis [five males and 35 females; age at examination: 41.5 ± 15.9 years (mean ± SD), range: 18–89] who were diagnosed with multiple sclerosis based on McDonald's diagnostic criteria (McDonald *et al.*, 2001) at the Department of Neurology, Kyushu University Hospital were enrolled in this study. In addition, 19 patients with spinocerebellar degeneration (SCD) (nine males and 10 females; age: 59.4 ± 10.9 years, range: 32–80) were used as controls. The multiple sclerosis patients were clinically classified into two subtypes: OS-multiple sclerosis and C-multiple sclerosis, as described previously (Kira *et al.*, 1996). Briefly, patients who showed a relapsing–remitting course and had both optic nerve and spinal cord involvement without any clinical evidence of disease in either the cerebrum or cerebellum were considered to have OS-multiple sclerosis. Patients who showed minor brainstem signs, such as transient double vision and nystagmus, in addition to opticospinal involvement, were included in this subtype. All other patients who showed multiple involvement of the CNS, including the cerebrum and cerebellum, were considered to have C-multiple sclerosis. The disability status of the patients was scored by one of the authors (T.I.) throughout the study, according to the EDSS (Kurtzke, 1983). The mean times from symptom onset to lumbar puncture (LP) were 13.9 days (range: 1–30 days) for OS-multiple sclerosis and 12.8 days (range: 1–30 days) for C-multiple sclerosis; the two did not differ significantly. Of the 40 multiple sclerosis patients, five C-multiple sclerosis and 10 OS-multiple sclerosis patients had received IFN-β or high-dose corticosteroids at the time of LP. The demographic features of the patients are summarized in Table 1. The ages at onset and LP, the EDSS score and CSF/serum albumin ratio were significantly higher in OS-multiple sclerosis than in C-multiple sclerosis ($P = 0.0000064$, 0.0000049, 0.019 and 0.023, respectively), while the disease duration, number of relapses, CSF cell count, total protein amount and IgG index did not differ significantly between the two.

For analysis of intracellular IFN-γ and IL-4 in CSF cells, 24 patients with multiple sclerosis (two males and 22 females; age: 45.2 ± 18.2 years, range: 21–89) who fulfilled McDonald's criteria and 12 control patients with various other non-inflammatory neurological diseases (seven males and five females; age: 52.4 ± 17.2 years, range: 20–75) were enrolled. In the multiple sclerosis group, 11 had OS-multiple sclerosis and 13 had C-multiple sclerosis. Of these, 21 were relapsing–remitting multiple sclerosis (11 OS-multiple sclerosis and 10 C-multiple sclerosis) and three were secondary progressive multiple sclerosis (three C-multiple sclerosis). The control group of 12 patients was comprised of two with amyotrophic lateral sclerosis, two with Alzheimer's disease, two with cervical spondylosis, one with SCD, one with Parkinson's disease, one with progressive supranuclear palsy, one with spinal cord infarction, one with epilepsy and one with conversion hysteria. The demographic features of the patients are also summarized in Table 1. The ages at onset and LP, and CSF/serum albumin ratio were significantly higher in OS-multiple sclerosis than in C-multiple sclerosis ($P = 0.017$, 0.028 and 0.028, respectively).

CSF sample collection

At least 5 ml of CSF was obtained from all patients by non-traumatic LP. Twenty-three CSF samples (all at the relapse phase) from 20 OS-multiple sclerosis patients, 22 CSF samples (all at the relapse phase) from 20 C-multiple sclerosis patients, and 19 CSF samples from 19 control patients were obtained for extracellular cytokine analysis. Neither multiple sclerosis nor control patients had any ongoing or recent infection at the time of LP. Intracellular IFN-γ and IL-4 analyses were performed using 11 CSF samples (10 at the relapse phase and one at the remission phase) from 11 OS-multiple sclerosis patients, 13 CSF samples (seven at the relapse phase, three at the remission phase and three at the progressive phase) from 13 C-multiple sclerosis patients, and 12 CSF samples from 12 control patients. CSF samples were immediately centrifuged at 800 r.p.m./min at 4°C for 5 min, and the supernatants stored at −70°C until analysis. The cell counts, total protein amounts, CSF/serum albumin ratio and IgG index used for the study are shown in Table 1.

Multiplexed fluorescent bead-based immunoassay

CSF supernatants were collected and analysed simultaneously for 16 different cytokines and chemokines, namely IL-1β, IL-2, IL-4, IL-5, IL-6, IL-7, IL-8, IL-10, IL-12 (p70), IL-13, IL-17, IFN-γ, TNF-α, G-CSF, MCP-1 and MIP-1β, using the Bio-Plex Cytokine Assay System (Bio-Rad Laboratories, Hercules, CA) according to the manufacturer's instructions (Kellar *et al.*, 2001; de Jager *et al.*, 2003). Briefly, 50 μl of each CSF supernatant and various concentrations of each cytokine standard (Bio-Rad) were added to 50 μl of antibody-conjugated beads (Bio-Rad) in a 96-well filter plate (Millipore, Billerica, MA). After a 30 min incubation, the plate was washed and 25 μl of a biotinylated antibody solution (Bio-Rad) was added to each well, followed by another 30 min incubation. The plate was then washed and 50 μl of streptavidin-conjugated phycoerythrin (PE; Bio-Rad) was added to each well and incubated for 10 min. Following a final wash, the contents of each well were resuspended in 125 μl of assay buffer (Bio-Rad) and analysed using a Bio-Plex Array Reader (Bio-Rad). The cytokine concentrations were calculated by reference to a standard curve for each cytokine derived using various concentrations of the cytokine standards (0.2, 0.78, 3.13, 12.5, 50, 200, 800 and 3200 pg/ml) assayed in the same manner as the CSF samples. The same lots of monoclonal antibodies for Bio-Plex Cytokine Assay System were used throughout the experiments, and the inter- and intra-assay variability was reported to be <10% (manufacturer's instructions). The detection limit of each cytokine was determined by the recovery of the corresponding cytokine standard, and the lowest values showing >50% recovery were set as the lower detection limits. The lower detection limit for each cytokine was as follows: 0.2 pg/ml for IL-2, IL-4, IL-5, IL-7, IL-8, IL-10, IL-12 (p70), IL-13, IL-17, IFN-γ and TNF-α, 0.78 pg/ml for IL-1β and IL-6, and 3.13 pg/ml for G-CSF, MCP-1 and MIP-1β. All samples were analysed undiluted in duplicate.

Intracellular cytokine analysis by flow cytometry

Each CSF supernatant was carefully removed and the cell sediment was suspended in RPMI 1640 (Nipro, Tokyo, Japan) supplemented with 10% fetal calf serum (FCS; Gibco BRL, Gaithersburg, MD; Lot # 3217341S), followed by incubation with 25 ng/ml phorbol 12-myristate 13-acetate (PMA; Sigma, St Louis, MO), 1.0 μg/ml ionomycin (Sigma) and 10 μg/ml brefeldin A (BFA; Sigma) in a 24-well plate at 37°C for 4 h under 5% CO_2. After washing with phosphate-buffered saline containing 0.1% bovine serum albumin (0.1% BSA–PBS), cells were stained with perCP-conjugated anti-CD4 monoclonal antibodies (Immunotech, Marseille, France) and incubated on ice in the dark for 15 min. Following another wash with 0.1% BSA–PBS, fluorescence-activated cell sorting (FACS) permeabilizing solution (Becton Dickinson, San Jose, CA) was added and the cells were placed in the dark for 10 min. After two washes with 0.1% BSA–PBS, the cells were stained with fluorescein isothiocyanate (FITC)-conjugated anti-IFN-γ (Immunotech) and PE-conjugated anti-IL-4 (Immunotech) antibodies for intracellular cytokine analysis, or with mouse IgG2a–FITC (Immunotech) and IgG1–PE (Immunotech) as controls, respectively. After a 30 min incubation on ice in the dark, the percentages of intracellular IFN-γ- and IL-4-producing cells were immediately analysed by flow cytometry using an Epics XL System II (Coulter, Hialeah, FL). Analysis gates were first set on lymphocytes according to the forward and side scatter properties and then on $CD4^+$ lymphocytes. Cases with a $CD4^+$ cell count of <500 were discarded from the analysis to increase the reliability.

Neuroimaging of the spinal cord

For spinal cord MRI, T2-weighted (SE 2500–4900/113–116) and T1-weighted (SE 400–500/11–12) images were obtained in the sagittal and axial planes. For the contrast-enhanced study, MRI was initiated 2–3 min after intravenous administration of gadolinium-pentetic acid (0.1 mmol/kg), using the T1-weighted sequences in the sagittal and axial planes. Lengths of spinal cord lesions were expressed in cm. Longitudinally extensive spinal cord lesions were defined as those extending over three vertebral spine lengths, which are considered to be exceptional in multiple sclerosis (McDonald *et al.*, 2001). Spinal cord MRIs taken at the time of relapse when the CSF samples were drawn (within 30 days of the onset of acute or subacute exacerbation) were evaluated independently by two examiners, of whom one (F.M.) was an experienced neuroradiologist and was blinded to the diagnosis. Spinal cord MRIs at the relapse were available for 34 of 40 multiple sclerosis patients (17 OS-multiple sclerosis and 17 C-multiple sclerosis patients) and, of these, 30 had spinal cord symptomatology (17 OS-multiple sclerosis and 13 C-multiple sclerosis).

Histopathological analysis of infiltrating cells in autopsied spinal cord specimens of OS-multiple sclerosis and C-multiple sclerosis

For the neuropathological analysis, spinal cord specimens obtained at autopsy from six OS-multiple sclerosis and two C-multiple sclerosis cases were used. Each autopsied specimen was fixed in 10% buffered formalin for several weeks, and then embedded in paraffin. Sections were either stained with haematoxylin and eosin, or immunostained using rabbit polyclonal antibodies against myeloperoxidase (1 : 500; NeoMarkers, Fremont, CA) or myelin basic protein (1 : 200; DAKO, Denmark) or mouse monoclonal antibodies against phosphorylated neurofilaments (1 : 200; DAKO; clone 2F11), macrophages (1 : 500; DAKO; clone KP1), T-cell antigen (1 : 500; DAKO; clone UCHL1) or B-cell antigen (1 : 500; DAKO; clone L26). Autoclave or microwave pre-treatment was performed to retrieve the antigens for immunostaining. The number of infiltrating cells, including neutrophils, macrophages, and T and B cells, was averaged for four separate fields (each field ×200) in the lesion in the same cross-section of the spinal cord.

Statistical analysis

Fisher's exact probability test was employed for comparisons of the detection rates of cytokines and chemokines in each group. The non-parametric Mann-Whitney *U* test was employed for comparison of the cytokine and chemokine levels in each group. The difference between PBLs and CSF in each group was analysed by Wilcoxon signed-rank test. Statistical significance was set at $P < 0.05$. Spearman's rank correlation analysis was used for statistical analysis of correlations between various clinical parameters and CSF cytokine levels.

Results

Detection rates of each cytokine and chemokine in CSF supernatants

The detection rate of IL-10 was significantly higher in OS-multiple sclerosis and C-multiple sclerosis patients than in control patients (91.3 versus 36.8%, $P = 0.00027$ in OS-multiple sclerosis; 81.8 versus 36.8%, $P = 0.0046$ in C-multiple sclerosis), while that of IL-7 was significantly lower in OS-multiple sclerosis and C-multiple sclerosis patients than in control patients (60.9 versus 100%, $P = 0.002$ in OS-multiple sclerosis; 68.2 versus 100%, $P = 0.0098$ in C-multiple sclerosis). In addition, IL-17 was significantly higher in OS-multiple sclerosis patients than in control patients (73.9 versus 36.8%, $P = 0.028$), while TNF-α was significantly higher in C-multiple sclerosis patients than in control patients (77.3 versus 42.1%, $P = 0.029$). The detection rates of other cytokines did not differ significantly between control patients and the two multiple sclerosis subtypes. When the five C-multiple sclerosis and 10 OS-multiple sclerosis patients on immunomodulatory therapies were excluded, essentially the same results were obtained, except that the increased detection rate of TNF-α in C-multiple sclerosis lost significance. IL-2 was not used for further statistical analysis because of its extremely low detection rate (<20% in total) in CSF.

Comparison among diseases of cytokine and chemokine levels in CSF supernatants

The cytokine and chemokine levels in CSF supernatants from controls, OS-multiple sclerosis and C-multiple sclerosis patients analysed by the multiplexed fluorescent bead-based immunoassay are shown in Fig. 1. Among the 16 cytokines examined, IL-17, MIP-1β, IL-13 and IL-1β were only significantly increased in OS-multiple sclerosis patients compared with control patients. IL-8, IL-10 and TNF-α were significantly increased in both OS-multiple sclerosis and C-multiple sclerosis patients compared with control patients. On the other hand, IL-7 and MCP-1 were significantly decreased in both OS-multiple sclerosis and C-multiple sclerosis patients compared with control patients. When the cytokine levels were compared between the two multiple sclerosis subtypes, IL-17, IL-8 and IL-5 were significantly increased in OS-multiple sclerosis patients compared with C-multiple sclerosis patients.

Considering the possibly low reliability for the lower ranges of the cytokine/chemokine concentrations (<1 pg/ml), we set 1 pg/ml as the cut-off level and reanalysed the data. Even when this cut-off level was used, the increased IL-17, MIP-1β, IL-13 and IL-1β in OS-multiple sclerosis patients, increased TNF-α in C-multiple sclerosis patients, increased IL-8 in both OS-multiple sclerosis and C-multiple sclerosis patients, decreased IL-7 in C-multiple sclerosis patients and decreased MCP-1 in both OS-multiple sclerosis and C-multiple sclerosis patients compared with control patients, and higher levels of IL-17, IL-8 and IL-5 in OS-multiple sclerosis patients than in C-multiple sclerosis patients were all still statistically significant. When the five C-multiple sclerosis and 10 OS-multiple sclerosis patients on immunomodulatory therapies were excluded, the increased IL-17 and MIP-1β in OS-multiple sclerosis patients, increased IL-8 in both OS-multiple sclerosis and C-multiple sclerosis patients, and decreased MCP-1 in C-multiple sclerosis patients compared with control patients, and higher levels of IL-17 in OS-multiple sclerosis patients than in C-multiple sclerosis patients still held statistical significance using this cut-off level. The statistical significances for the cytokine/chemokine changes are summarized in Table 2 according to cut-off level and the presence or absence of immunomodulatory therapies.

Comparison of the intracellular cytokine production in CD4$^+$ T cells between CSF and PBLs and among diseases

IFN-γ$^+$IL-4$^-$ CD4$^+$ T-cell percentages were significantly higher in CSF cells than in PBLs for all three groups (Fig. 2). In PBLs, there were no significant differences in the IFN-γ$^+$IL-4$^-$ CD4$^+$ T-cell percentages among the three groups, while in CSF cells, IFN-γ$^+$IL-4$^-$ CD4$^+$ T-cell percentages were significantly increased in both OS-multiple sclerosis and C-multiple sclerosis patients compared with control patients. For the IFN-γ$^-$IL-4$^+$ CD4$^+$ T-cell percentages, CSF cells only showed a significantly lower value than PBLs in control patients. There was no significant change in the IFN-γ$^-$IL-4$^+$ T-cell percentages between PBLs and CSF cells in either OS-multiple sclerosis or C-multiple sclerosis patients, and in OS-multiple sclerosis patients, CSF cells even showed a higher IFN-γ$^-$IL-4$^+$ T-cell percentage than PBLs. In PBLs, IFN-γ$^-$IL-4$^+$ CD4$^+$ T-cell percentages were significantly decreased in OS-multiple sclerosis and C-multiple sclerosis patients compared with control patients. In CSF cells, IFN-γ$^-$IL-4$^+$ CD4$^+$ T-cell percentages did not differ significantly between control and OS-multiple sclerosis patients, while C-multiple sclerosis patients had a significantly lower IFN-γ$^-$IL-4$^+$ CD4$^+$ T-cell percentage than OS-multiple sclerosis patients, and showed a lower value than control patients although the difference was not significant.

Consequently, the intracellular IFN-γ/IL-4 ratio in CD4$^+$ T cells was significantly higher in CSF cells than in PBLs in

Table 2 *Summary of cytokine/chemokine changes in CSF supernatants*

	Altered cytokine/chemokine	All samples	⩾1 pg/ml*	⩾1 pg/ml*, no immunomodulatory drugs
OS-multiple sclerosis versus control	IL-17	↑ $P = 0.0031$	↑ $P = 0.0038$	↑ $P = 0.0093$
	IL-8	↑ $P = 0.000009$	↑ $P = 0.000009$	↑ $P = 0.0014$
	MIP-1β	↑ $P = 0.0042$	↑ $P = 0.0042$	↑ $P = 0.024$
	IL-1β	↑ $P = 0.027$	↑ $P = 0.039$	NS
	IL-13	↑ $P = 0.027$	↑ $P = 0.022$	NS
	IL-10	↑ $P = 0.000051$	NS	NS
	TNF-α	↑ $P = 0.026$	NS	NS
	MCP-1	↓ $P = 0.04$	↓ $P = 0.04$	NS
	IL-7	↓ $P = 0.0048$	NS	NS
C-multiple sclerosis versus control	IL-8	↑ $P = 0.0012$	↑ $P = 0.0012$	↑ $P = 0.015$
	TNF-α	↑ $P = 0.0055$	↑ $P = 0.015$	NS
	IL-10	↑ $P = 0.00054$	NS	NS
	MCP-1	↓ $P = 0.034$	↓ $P = 0.034$	↓ $P = 0.024$
	IL-7	↓ $P = 0.000053$	↓ $P = 0.013$	NS
OS-multiple sclerosis versus C-multiple sclerosis	IL-17	↑ $P = 0.045$	↑ $P = 0.024$	↑ $P = 0.028$
	IL-8	↑ $P = 0.029$	↑ $P = 0.029$	NS
	IL-5	↑ $P = 0.0048$	↑ $P = 0.0051$	NS

NS = not significant; ↑ = elevated; ↓ = decreased. *The cut-off level was 1 pg/ml.

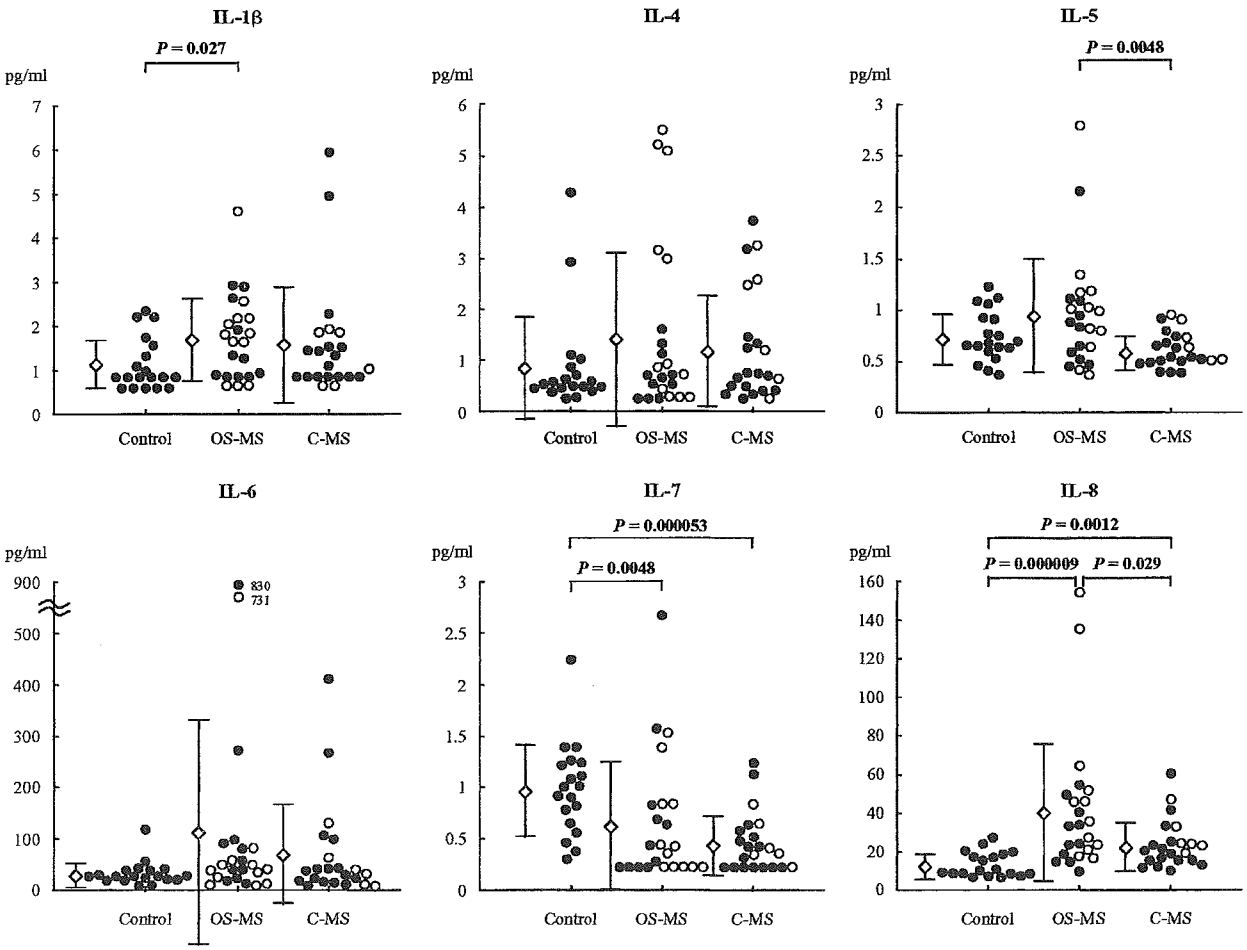

Fig. 1 Continued.

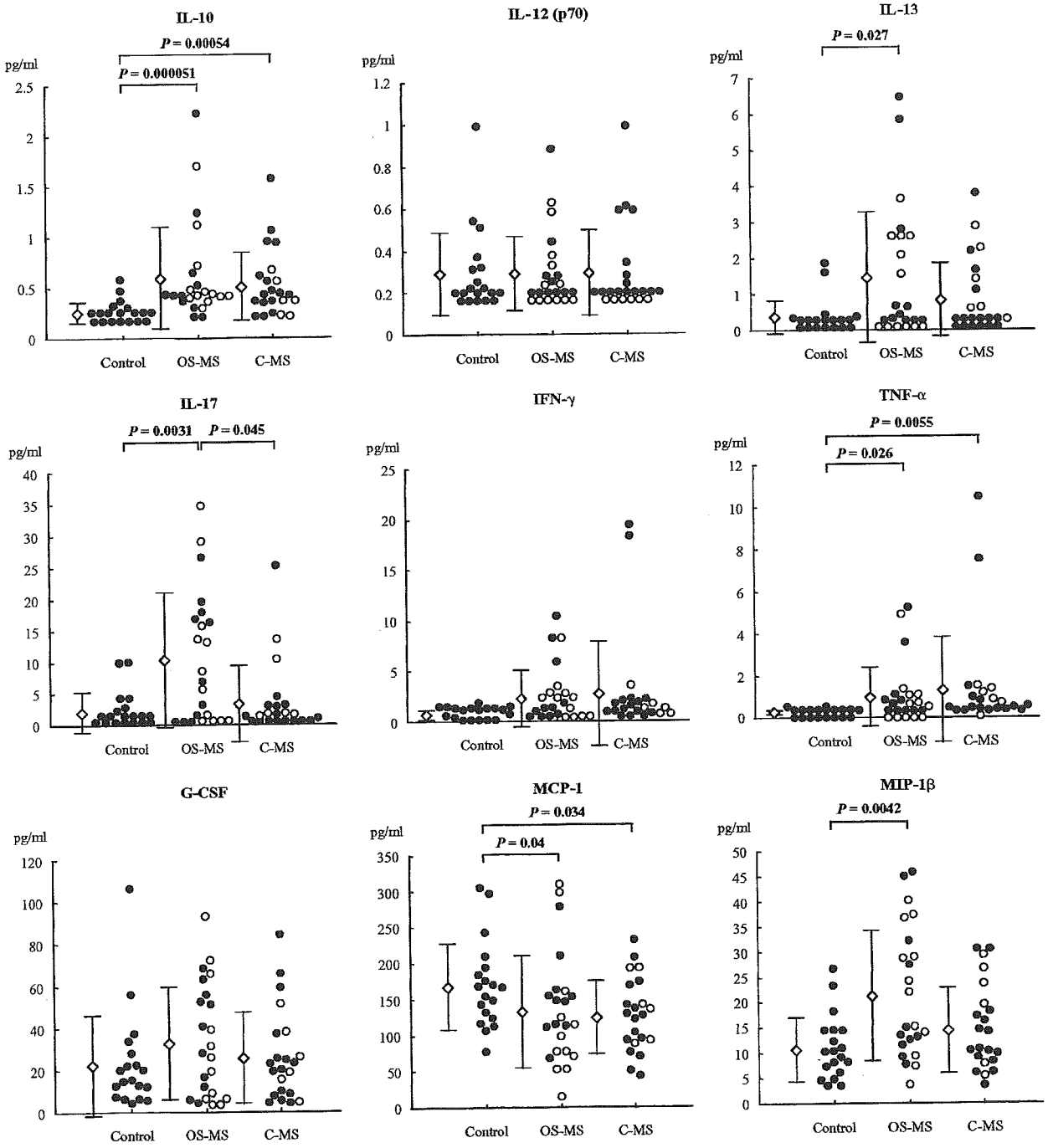

Fig. 1 Cytokine and chemokine levels in CSF supernatants from patients with SCD (controls), OS-multiple sclerosis and C-multiple sclerosis assessed by the multiplexed fluorescent bead-based immunoassay. There were 47 samples in total: 19 controls, 23 OS-multiple sclerosis and 22 C-multiple sclerosis. Multiple sclerosis samples were all obtained from patients at relapse. Open circles indicate patients who were under immunomodulatory therapies (12 OS-multiple sclerosis and six C-multiple sclerosis samples), while closed circles indicate those who were not (11 OS-multiple sclerosis and 16 C-multiple sclerosis samples). IL-2 is not shown due to its low detection frequency in CSF. Open diamonds and bars indicate the mean ± SD for each group.

both control and C-multiple sclerosis patients, while it did not differ significantly between CSF cells and PBLs in OS-multiple sclerosis patients. In PBLs, the ratio was significantly elevated in both OS-multiple sclerosis and C-multiple sclerosis patients compared with control patients, whereas in CSF cells, the ratio was significantly increased only in C-multiple sclerosis and not OS-multiple sclerosis patients. IFN-γ^+IL-4^+ $CD4^+$ T-cell percentages were significantly

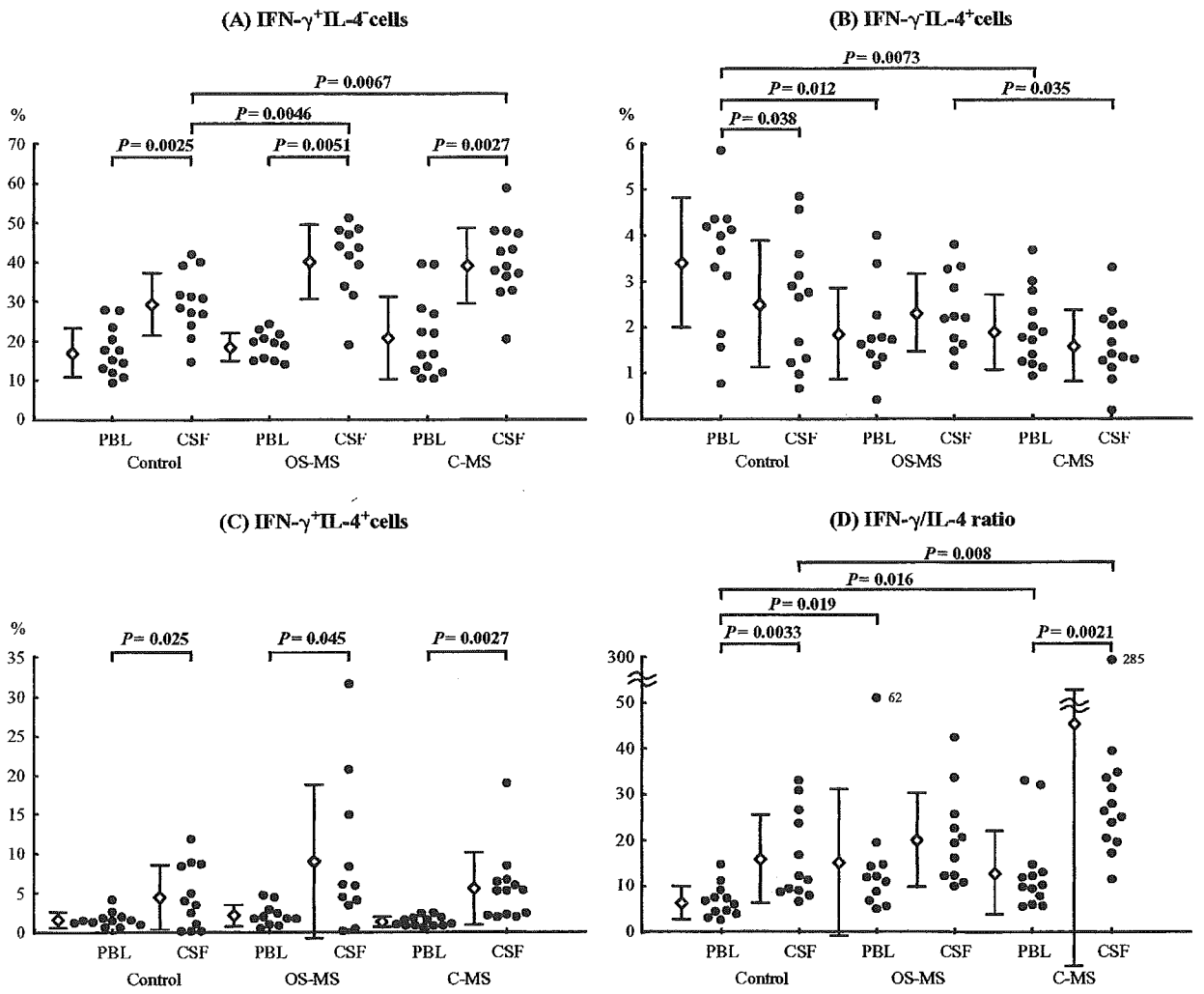

Fig. 2 Intracellular cytokine production patterns of PBLs and CSF $CD4^+$ T cells from OND (other non-inflammatory neurological diseases; control), OS-multiple sclerosis and C-multiple sclerosis patients. (**A**) IFN-γ^+IL-4^- $CD4^+$ T-cell percentages. (**B**) IFN-γ^-IL-4^+ $CD4^+$ T-cell percentages. (**C**) IFN-γ^+IL-4^+ $CD4^+$ T-cell percentages. (**D**) Intracellular IFN-γ/IL-4 ratios in $CD4^+$ T cells. There were 36 samples in total: 12 controls, 11 OS-multiple sclerosis and 13 C-multiple sclerosis. Open diamonds and bars indicate the mean ± SD for each group.

higher in CSF cells than in PBLs in all three groups. IFN-γ^+IL-4^+ $CD4^+$ T-cell percentages did not differ significantly among control, OS-multiple sclerosis and C-multiple sclerosis patients in either PBLs or CSF cells.

Neuroimaging findings of spinal cord

Longitudinally extensive spinal cord lesions (Fig. 3) were found in 17 of 34 (50.0%) multiple sclerosis patients around the time their CSF was examined. The frequency of longitudinally extensive spinal cord lesions was higher in OS-multiple sclerosis than in C-multiple sclerosis (12 out of 17, 70.6 versus five out of 17, 29.4%, $P = 0.038$). In addition, the spinal cord lesions were also longer in OS-multiple sclerosis than in C-multiple sclerosis (5.5 ± 3.1 versus 2.7 ± 3.3 cm, $P = 0.021$).

Correlations between clinical parameters and cytokine levels in CSF supernatants in multiple sclerosis

Among the cytokines/chemokines elevated in multiple sclerosis CSF supernatants, only IL-8 showed a significant correlation with the EDSS score (Kurtzke, 1983) in multiple sclerosis (Fig. 4). Significant positive correlations with the CSF/serum albumin ratio as well as CSF protein concentration were found for IL-8 and IL-17. Moreover, lengths of spinal cord lesions on MRI significantly correlated with IL-8 and IL-17 levels. Multiple sclerosis patients with longitudinally extensive spinal cord lesions on MRI (>3 vertebral length) had significantly higher levels of IL-8 and IL-17 than those without such lesions [49.23 ± 38.36 versus 16.35 ± 6.08 pg/ml (mean ± SD], $P = 0.000039$ for IL-8; 13.35 ± 11.43 versus 2.70 ± 4.97 pg/ml (mean ± SD),

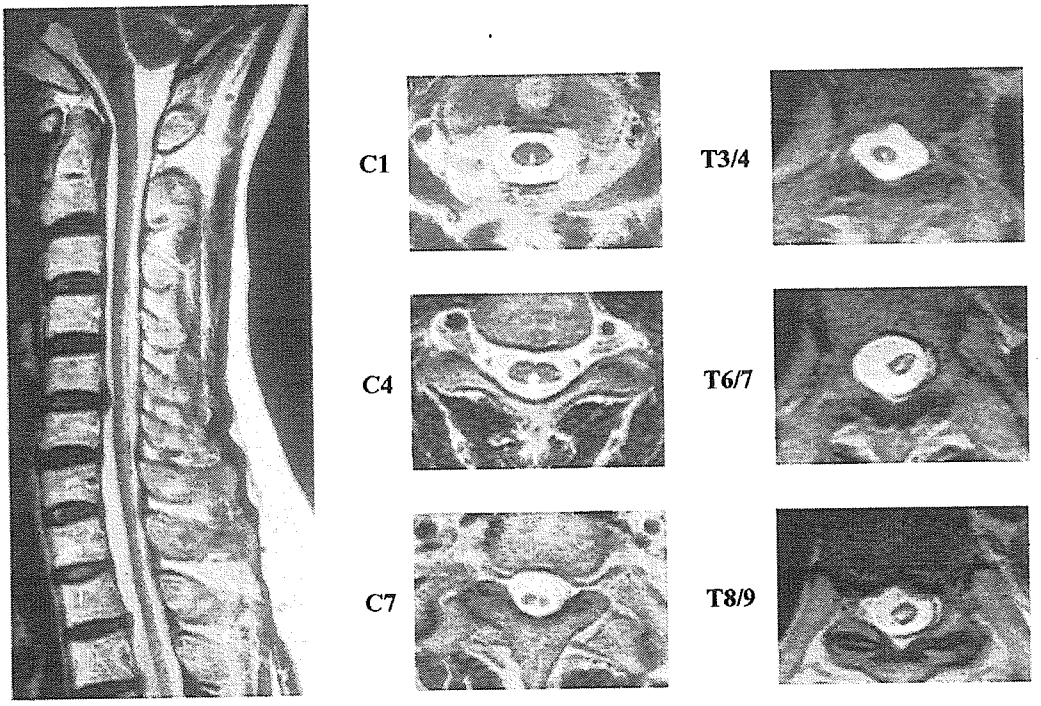

Fig. 3 Representative longitudinally extensive spinal cord MRI lesions on T2-weighted images from a 52-year-old patient with OS-multiple sclerosis at relapse.

$P = 0.0018$ for IL-17]. No other clinical parameters, such as age at onset, age at examination, disease duration, sex or clinical course, showed any significant correlation with the CSF supernatant cytokine/chemokine levels. Even when the five C-multiple sclerosis and 10 OS-multiple sclerosis patients on immunomodulatory therapies were excluded, essentially the same correlations were obtained.

Histopathological analysis of infiltrating cells in autopsied specimens of OS-multiple sclerosis and C-multiple sclerosis

We examined spinal cord specimens obtained at autopsy from six OS-multiple sclerosis and two C-multiple sclerosis cases. Of these, prominent CSF neutrophilia was noted in two of the five OS-multiple sclerosis cases whose CSF records were available. Their demographic features and neuropathological findings are summarized in Table 3. In the OS-multiple sclerosis cases, the spinal cord lesions extended over the white matter to the grey matter, and all the cases showed moderate to severe myelin and axonal damage, indicating so-called necrotic lesions. In the lesions, macrophage infiltration was universal in all cases, and was severe in three, moderate in one and mild in two. Numerous lymphocytes, mostly consisting of T lymphocytes, infiltrated either the perivascular area or parenchyma. In addition, three cases showed neutrophilic infiltration in both the grey and white matter of the spinal cord. Regarding the neutrophil infiltration, either focal accumulation or a diffuse scattered pattern was seen. In particular, focal neutrophil accumulation was noted around vessel walls or in parenchyma in two cases (Fig. 5). However, we found no eosinophil infiltration in any of the lesions by haematoxylin–eosin staining. Although the spinal cord lesions in one of the two C-multiple sclerosis cases showed severe necrosis with macrophage infiltration, infiltration of neutrophils was not evident in either of these C-multiple sclerosis cases.

Discussion

In the present study, although the numbers of CSF samples at relapse were limited due to the rarity of multiple sclerosis in Japanese and the popular use of immunomodulatory drugs, we successfully uncovered subtype-related CSF cytokine/chemokine changes in multiple sclerosis, since upregulation of the neutrophil-recruiting IL-17/IL-8 axis was characteristic for OS-multiple sclerosis and correlated with the development of longitudinally extensive spinal cord lesions. Furthermore, we have directly shown that in CSF cells, IFN-γ^+IL-4$^-$ CD4$^+$ T cells are increased in both OS-multiple sclerosis and C-multiple sclerosis, while IFN-γ^-IL-4$^+$ CD4$^+$ T cells are significantly more abundant in OS-multiple sclerosis than in C-multiple sclerosis, even at relapse.

Cytokine analysis at the cellular level in CSF has been difficult because of the extreme fragility and limited numbers of CSF cells. In the current study, however, our method successfully measured the intracellular cytokine production

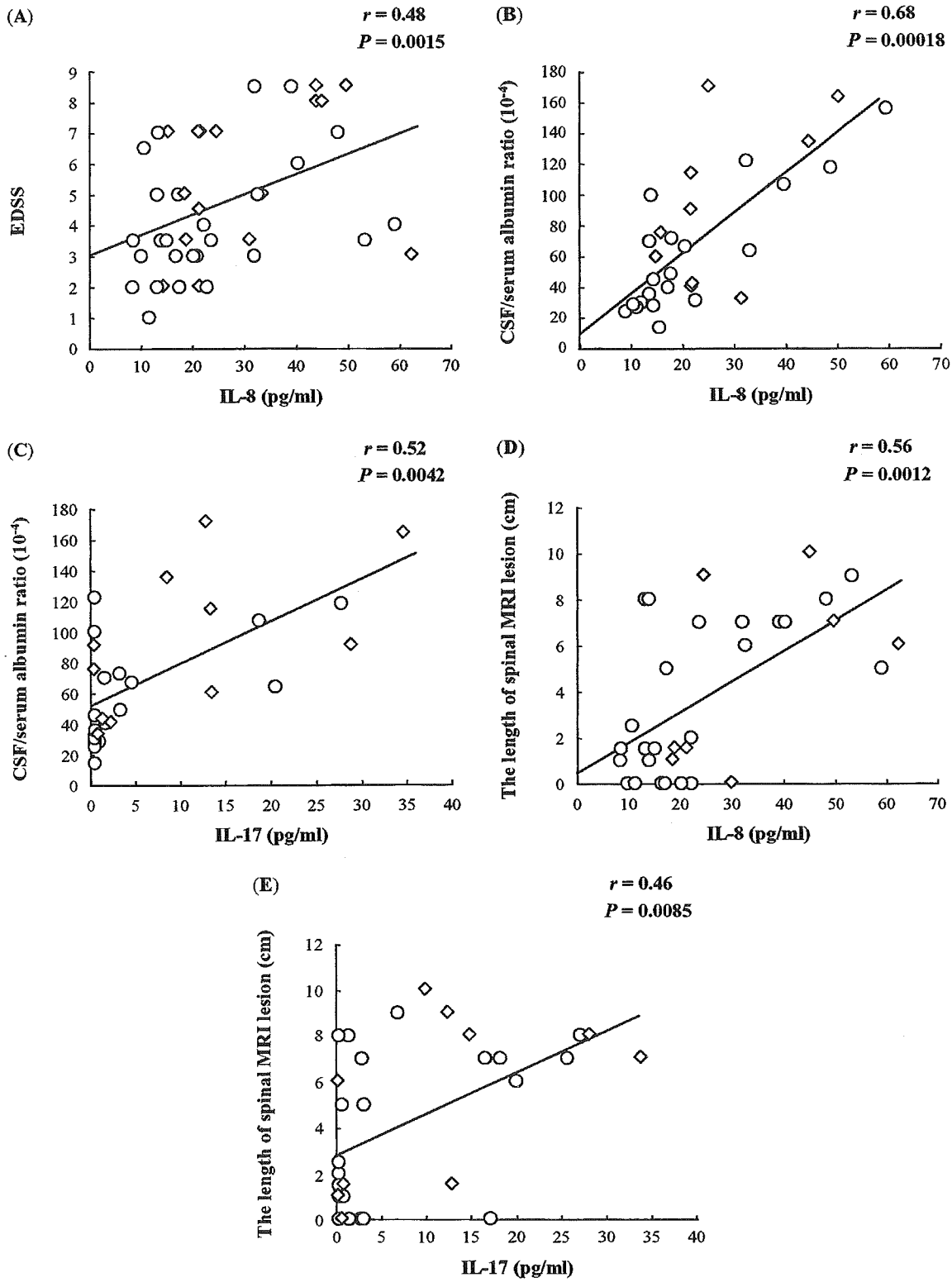

Fig. 4 Correlations between various clinical parameters and the cytokine/chemokine levels in CSF supernatants. (**A**) EDSS scores and IL-8 levels. (**B**) CSF/serum albumin ratio and IL-8 levels. The CSF protein concentration was also significantly correlated with IL-8 (r = 0.56, P = 0.00026, data not shown in the figure). (**C**) CSF/serum albumin ratio and IL-17 levels. The CSF protein concentration was also significantly correlated with IL-17 (r = 0.53, P = 0.00054, data not shown in the figure). (**D**) Length of spinal cord MRI lesions and IL-8 levels. (**E**) Length of spinal cord MRI lesions and IL-17 levels. Open diamonds indicate patients who were under immunomodulatory therapies, while open circles indicate those who were not.